Unusual Otto excitation dynamics and enhanced coupling of light to TE plasmons in graphene

Daniel R. Mason, Sergey G. Menabde, and Namkyoo Park[*]

Photonic Systems Laboratory, School of EECS, Seoul National University, Seoul 151-744, South Korea
[*]*nkpark@snu.ac.kr*

Abstract: Transverse-electric (TE) plasmons are a unique and unusual aspect of graphene's plasmonic response that are predicted to manifest when the sign of imaginary part of conductivity changes to negative near the spectral onset of interband transitions. Although thus far, a feasible platform for the direct experimental detection of TE plasmons at finite temperature is yet to be suggested. Here we analyze the dynamics of Otto-Kretschmann excitation of TE plasmons in graphene. We show that TE plasmons supported by graphene in an Otto configuration unusually exhibit a cutoff thickness between the coupling prism and the graphene layer that forbids their efficient coupling to an incident wave in the case of a single-layer graphene at typical finite temperatures. In contrast, significantly increased coupling in the case of an *N*-layer graphene insulator stack, owing to an *N*-fold increase of the effective graphene conductivity as the insulator thickness approaches zero, is predicted to provide a TE plasmon resonance that is easily detectable at room temperature.

References and links

1. A. K. Geim, "Graphene: status and prospects," Science **324**(5934), 1530–1534 (2009).
2. K. S. Novoselov, A. K. Geim, S. V. Morozov, D. Jiang, Y. Zhang, S. V. Dubonos, I. V. Grigorieva, and A. A. Firsov, "Electric field effect in atomically thin carbon films," Science **306**(5696), 666–669 (2004).
3. A. H. Castro Neto, F. Guinea, N. M. R. Peres, K. S. Novoselov, and A. K. Geim, "The electronic properties of graphene," Rev. Mod. Phys. **81**(1), 109–162 (2009).
4. F. Bonaccorso, Z. Sun, T. Hasan, and A. C. Ferrari, "Graphene photonics and optoelectronics," Nat. Photonics **4**(9), 611–622 (2010).
5. A. N. Grigorenko, M. Polini, and K. S. Novoselov, "Graphene plasmonics," Nat. Photonics **6**(11), 749–758 (2012).
6. F. Wang, Y. Zhang, C. Tian, C. Girit, A. Zettl, M. Crommie, and Y. R. Shen, "Gate-Variable Optical Transitions in Graphene," Science **320**(5873), 206–209 (2008).
7. Q. Bao, H. Zhang, Y. Wang, Z. Ni, Y. Yan, Z. X. Shen, K. P. Loh, and D. Y. Tang, "Atomic-layer graphene as a saturable absorber for ultrafast pulsed lasers," Adv. Funct. Mater. **19**(19), 3077–3083 (2009).
8. R. R. Nair, P. Blake, A. N. Grigorenko, K. S. Novoselov, T. J. Booth, T. Stauber, N. M. R. Peres, and A. K. Geim, "Fine structure constant defines visual transparency of graphene," Science **320**(5881), 1308 (2008).
9. Y. W. Song, S. Y. Jang, W. S. Han, and M. K. Bae, "Graphene mode-lockers for fiber lasers functioned with evanescent field interaction," Appl. Phys. Lett. **96**(5), 051122 (2010).
10. A. Y. Nikitin, F. Guinea, F. J. Garcia-Vidal, and L. Martin-Moreno, "Surface plasmon enhanced absorption and suppressed transmission in periodic arrays of graphene ribbons," Phys. Rev. B **85**(8), 081405(R) (2012).
11. R. Alaee, M. Farhat, C. Rockstuhl, and F. Lederer, "A perfect absorber made of a graphene micro-ribbon metamaterial," Opt. Express **20**(27), 28017–28024 (2012).
12. S. Thongrattanasiri, F. H. L. Koppens, and F. J. García de Abajo, "Complete optical absorption in periodically patterned graphene," Phys. Rev. Lett. **108**(4), 047401 (2012).
13. G. Pirruccio, L. Martín Moreno, G. Lozano, and J. Gómez Rivas, "Coherent and broadband enhanced optical absorption in graphene," ACS Nano **7**(6), 4810–4817 (2013).
14. F. Xia, T. Mueller, Y. M. Lin, A. Valdes-Garcia, and P. Avouris, "Ultrafast graphene photodetector," Nat. Nanotechnol. **4**(12), 839–843 (2009).
15. X. Wang, Z. Cheng, K. Xu, H. K. Tsang, and J. B. Xu, "High-responsivity graphene/silicon-heterostructure waveguide photodetectors," Nat. Photonics **7**(11), 888–891 (2013).

16. A. Pospischil, M. Humer, M. M. Furchi, D. Bachmann, R. Guider, T. Fromherz, and T. Mueller, "CMOS-compatible graphene photodetector covering all optical communication bands," Nat. Photonics **7**(11), 892–896 (2013).
17. X. Gan, R. J. Shiue, Y. Gao, I. Meric, T. F. Heinz, K. Shepard, J. Hone, S. Assefa, and D. Englund, "Chip-integrated ultrafast graphene photodetector with high responsivity," Nat. Photonics **7**(11), 883–887 (2013).
18. M. Liu, X. Yin, E. Ulin-Avila, B. Geng, T. Zentgraf, L. Ju, F. Wang, and X. Zhang, "A graphene-based broadband optical modulator," Nature **474**(7349), 64–67 (2011).
19. M. Liu, X. Yin, and X. Zhang, "Double-layer graphene optical modulator," Nano Lett. **12**(3), 1482–1485 (2012).
20. C. C. Lee, S. Suzuki, W. Xie, and T. R. Schibli, "Broadband graphene electro-optic modulators with sub-wavelength thickness," Opt. Express **20**(5), 5264–5269 (2012).
21. S. J. Koester and M. Li, "High-speed waveguide-coupled graphene-on-graphene optical modulators," Appl. Phys. Lett. **100**(17), 171107 (2012).
22. S. H. Lee, M. Choi, T. T. Kim, S. Lee, M. Liu, X. Yin, H. K. Choi, S. S. Lee, C. G. Choi, S. Y. Choi, X. Zhang, and B. Min, "Switching terahertz waves with gate-controlled active graphene metamaterials," Nat. Mater. **11**(11), 936–941 (2012).
23. F. Xing, Z. B. Liu, Z. C. Deng, X. T. Kong, X. Q. Yan, X. D. Chen, Q. Ye, C. P. Zhang, Y. S. Chen, and J. G. Tian, "Sensitive real-time monitoring of refractive indexes using a novel graphene-based optical sensor," Sci Rep **2**, 908 (2012).
24. Q. Bao, H. Zhang, B. Wang, Z. Ni, C. H. Y. X. Lim, Y. Wang, D. Y. Tang, and K. P. Loh, "Broadband graphene polarizer," Nat. Photonics **5**(7), 411–415 (2011).
25. Y. V. Bludov, M. I. Vasilevskiy, and N. M. R. Peres, "Tunable graphene-based polarizer," J. Appl. Phys. **112**(8), 084320 (2012).
26. L. Ju, B. Geng, J. Horng, C. Girit, M. Martin, Z. Hao, H. A. Bechtel, X. Liang, A. Zettl, Y. R. Shen, and F. Wang, "Graphene plasmonics for tunable terahertz metamaterials," Nat. Nanotechnol. **6**, 630–634 (2011).
27. H. Yan, X. Li, B. Chandra, G. Tulevski, Y. Wu, M. Freitag, W. Zhu, P. Avouris, and F. Xia, "Tunable infrared plasmonic devices using graphene/insulator stacks," Nat. Nanotechnol. **7**(5), 330–334 (2012).
28. F. H. L. Koppens, D. E. Chang, and F. J. García de Abajo, "Graphene plasmonics: A platform for strong light-matter interactions," Nano Lett. **11**(8), 3370–3377 (2011).
29. C. Cocchi, D. Prezzi, A. Ruini, E. Benassi, M. J. Caldas, S. Corni, and E. Molinari, "Optical excitations and field enhancement in short graphene nanoribbons," J. Phys. Chem. Lett. **3**(7), 924–929 (2012).
30. S. Thongrattanasiri and F. J. García de Abajo, "Optical field enhancement by strong plasmon interaction in graphene nanostructures," Phys. Rev. Lett. **110**(18), 187401 (2013).
31. V. W. Brar, M. S. Jang, M. Sherrott, J. J. Lopez, and H. A. Atwater, "Highly confined tunable mid-infrared plasmonics in graphene nanoresonators," Nano Lett. **13**(6), 2541–2547 (2013).
32. M. Jablan, H. Buljan, and M. Soljačić, "Plasmonics in graphene at infrared frequencies," Phys. Rev. B **80**(24), 245435 (2009).
33. J. Chen, M. Badioli, P. Alonso-González, S. Thongrattanasiri, F. Huth, J. Osmond, M. Spasenović, A. Centeno, A. Pesquera, P. Godignon, A. Z. Elorza, N. Camara, F. J. García de Abajo, R. Hillenbrand, and F. H. L. Koppens, "Optical nano-imaging of gate-tunable graphene plasmons," Nature **487**(7405), 77–81 (2012).
34. Z. Fei, A. S. Rodin, G. O. Andreev, W. Bao, A. S. McLeod, M. Wagner, L. M. Zhang, Z. Zhao, M. Thiemens, G. Dominguez, M. M. Fogler, A. H. Castro Neto, C. N. Lau, F. Keilmann, and D. N. Basov, "Gate-tuning of graphene plasmons revealed by infrared nano-imaging," Nature **487**(7405), 82–85 (2012).
35. G. W. Hanson, "Dyadic Green's functions and guided surface waves for a surface conductivity model of graphene," J. Appl. Phys. **103**(6), 064302 (2008).
36. G. W. Hanson, A. B. Yakovlev, and A. Mafi, "Excitation of discrete and continuous spectrum for a surface conductivity model of graphene," J. Appl. Phys. **110**(11), 114305 (2011).
37. S. A. Mikhailov and K. Ziegler, "New electromagnetic mode in graphene," Phys. Rev. Lett. **99**(1), 016803 (2007).
38. M. Jablan, H. Buljan, and M. Soljačić, "Transverse electric plasmons in bilayer graphene," Opt. Express **19**(12), 11236–11241 (2011).
39. P. Yeh, *Optical Waves in Layered Media* (John Wiley & Sons, Inc., , 2005), Chap. 11.
40. O. V. Kotov, M. A. Kol'chenko, and Y. E. Lozovik, "Ultrahigh refractive index sensitivity of TE-polarized electromagnetic waves in graphene at the interface between two dielectric media," Opt. Express **21**(11), 13533–13546 (2013).
41. G. Gómez-Santos and T. Stauber, "Fluorescence quenching in graphene: A fundamental ruler and evidence for transverse plasmons," Phys. Rev. B **84**(16), 165438 (2011).
42. A. Yu. Nikitin, F. Guinea, F. J. Garcia-Vidal, and L. Martin-Moreno, "Fields radiated by a nanoemitter in a graphene sheet," Phys. Rev. B **84**(19), 195446 (2011).
43. A. Gutiérrez-Rubio, T. Stauber, and F. Guinea, "Transverse current response of graphene at finite temperature, plasmons and absorption," arXiv:1307.2024 (2013).
44. A. Otto, "Excitation of nonradiative surface waves in silver by the method of frustrated total reflection," Z. Phys. **216**(4), 398–410 (1968).
45. Yu. V. Bludov, A. Ferreira, N. M. R. Peres, and M. I. Vasilevskiy, "A primer on surface plasmon-polaritons in graphene," Int. J. Mod. Phys. B **27**(10), 1341001 (2013).

46. J. Hass, F. Varchon, J. E. Millán-Otoya, M. Sprinkle, N. Sharma, W. A. de Heer, C. Berger, P. N. First, L. Magaud, and E. H. Conrad, "Why multilayer graphene on 4H-SiC(0001[over]) behaves like a single sheet of graphene," Phys. Rev. Lett. **100**(12), 125504 (2008).
47. I. H. Baek, K. J. Ahn, B. J. Kang, S. Bae, B. H. Hong, D. I. Yeom, K. Lee, Y. U. Jeong, and F. Rotermund, "Terahertz transmission and sheet conductivity of randomly stacked multi-layer graphene," Appl. Phys. Lett. **102**(19), 191109 (2013).
48. M. A. K. Othman, C. Guclu, and F. Capolino, "Graphene–dielectric composite metamaterials: evolution from elliptic to hyperbolic wavevector dispersion and the transverse epsilon-near-zero condition," J. Nanophotonics **7**(1), 073089 (2013).
49. B. Wunsch, T. Stauber, F. Sols, and F. Guinea, "Dynamical polarization of graphene at finite doping," New J. Phys. **8**(12), 318 (2006).
50. E. H. Hwang and S. Das Sarma, "Dielectric function, screening, and plasmons in two-dimensional graphene," Phys. Rev. B **75**(20), 205418 (2007).
51. L. A. Falkovsky, "Optical properties of graphene," J. Phys. Conf. Ser. **129**, 012004 (2008).
52. E. Y. Yeatman, "Resolution and sensitivity in surface plasmon microscopy and sensing," Biosens. Bioelectron. **11**(6-7), 635–649 (1996).
53. M. L. Gorodetsky and V. S. Ilchenko, "Optical microsphere resonators: optimal coupling to high-Q whispering-gallery modes," J. Opt. Soc. Am. B **16**(1), 147–154 (1999).
54. R. Naraoka and K. Kajikawa, "Phase detection of surface plasmon resonance using rotating analyzer method," Sensor Actuat. Biol. Chem. **107**, 952–956 (2005).
55. J. Homola and M. Piliarik, "Surface Plasmon Resonance (SPR) Sensors," in *Surface Plasmon Resonance Based Sensors*, J. Homola, ed. (Springer, 2006).

1. Introduction

Graphene is an atomically thin hexagonal crystal of carbon atoms that has attracted overwhelming inter-disciplinary interest [1] since the initial demonstration of its large DC electrical conductivity that is tunable in real-time by electrical gating [2]. The outstanding electrical properties of graphene make it a candidate material for next generation electronic devices, and the unusual (linear) dispersion of its charge carriers makes it a unique test bed for exotic fundamental predictions of solid state theory [3]. Meanwhile, the results of numerous studies of graphene's electrodynamic response have led to an increasing interest in graphene from the optics and photonics communities for a variety of applications [4,5]. A unique and attractive feature of graphene's electrodynamic response is its tunability [6] between two different behaviors according to the Fermi energy of its charge carriers (E_F) relative to the photon energy ($\hbar\omega$). At small doping (or, high frequency; $\hbar\omega > 2E_F$), graphene exhibits a broadband and saturable [7] absorbance of ~2.3% [8] which has seen it implemented in mode-locked lasers [7,9], efficient absorbers [10–13], photo-detectors [14–17], modulators [18–22], optical sensors [23] and polarizers [24,25]. At large doping (or, low frequency; $\hbar\omega < 2E_F$), graphene responds as an atomically-thin Drude-metal which supports localized [12,26–31] and transverse-magnetic (TM) propagating [32–36] surface plasmon-polaritons (SPPs) with exceptionally strong electric field confinement.

On the other hand, studies focusing on graphene's spectral transition region ($\hbar\omega \sim 2E_F$) are surprisingly limited. Interestingly, in the spectral transition region, it has been predicted that the imaginary part of graphene's conductivity ($\mathrm{Im}[\sigma] = \sigma''$) changes sign from positive ($\sigma'' > 0$, i.e. metallic) at low frequencies, to negative ($\sigma'' < 0$, i.e. dielectric) at high frequencies [37]. Notably, this sign change has been associated with the predicted manifestation of transverse electric (TE) plasmons, rather than the conventional TM plasmons, i.e., TE (TM) for when $\sigma'' < 0$ ($\sigma'' > 0$), in both single- [37] and bi-layer [38] graphene. In analogy with the fundamental guided mode of a high-index dielectric slab waveguide [39] as the slab thickness approaches zero, TE plasmons supported by graphene are weakly bound [37] to the graphene plane, but exhibit very low propagation loss [37], and are highly sensitive to the optical contrast between adjacent dielectrics sandwiching the graphene layer [40]. Based on this sensitivity, a TE-plasmonic gas-sensor was recently proposed and predicted theoretically to exhibit an impressive detection limit exceeding 6.7×10^{-7} RIU (refractive index units) at room temperature [40]. However, the very existence of TE plasmons, which is a fundamental aspect of graphene's plasmonic response, is yet to be experimentally demonstrated. While theoretical

studies of TE plasmon-induced fluorescence rate modification [41,42] and the graphene susceptibility loss function [43] have suggested that experimental detection of TE plasmons will be a challenge due to weak coupling at finite temperatures, a thorough quantitative analysis pertaining to a real experimental setup is yet to be presented.

In this paper we study the dynamics of Otto-Kretschmann [44,45] excitation of TE plasmons in graphene as a route to their experimental detection. An Otto-Kretschmann (or simply, Otto) configuration, which has been ubiquitously employed for detection and measurement of SPPs on bulk metals, would allow the direct optical probing of TE plasmons, in contrast to indirect probing by secondary effects such as plasmon-induced modification of fluorescent decay rate. Furthermore, in contrast with the graphene TM plasmons that usually exhibit exceptionally large effective index [32,45], the small effective index of TE plasmons (close to that of the surrounding bulk [37]) should make them easily accessible to Otto excitation.

Our analytical and numerical investigation reveals the unusual existence of a cutoff film thickness between the coupling prism and the graphene layer - inversely proportional to the imaginary part of the graphene conductivity - below which TE plasmons in an Otto configuration are no longer fully bound to the graphene plane. It is found that, at realistic values of the conductivity of single-layer graphene at a temperature $T = 300$K and down to $T = 80$K, a large cutoff thickness combined with small plasmon propagation loss prevents efficient coupling of the incident wave to the TE plasmon, thus presenting a challenge to their experimental detection. As a route to improved detectability of TE plasmons, we propose and demonstrate that the experimental conditions could be significantly relaxed by introducing multi-layer graphene stacks [27,46–48].

2. Conductivity of graphene in the spectral transition region at finite temperature

The sheet conductivity of single-layer graphene is obtained from the random phase approximation (RPA) [32,49,50] in the local limit, $q \rightarrow 0$ (or, $q \ll k_F$; q is the plasmon wavenumber, and k_F is the Fermi wavenumber) [51]:

$$\sigma(\omega) = \ln\left[2\cosh\left(\frac{E_F}{2k_B T}\right)\right]\frac{2e^2 k_B T}{\pi\hbar^2}\frac{i}{\omega + i/\tau} + \frac{e^2}{4\hbar}\left\{H(\omega/2) + \frac{4i\omega}{\pi}\int_0^\infty dx \frac{H(x) - H(\omega/2)}{\omega^2 - 4x^2}\right\},$$

(1)

where

$$H(x) = \frac{\sinh(\hbar x / k_B T)}{\cosh(E_F / k_B T) + \cosh(\hbar x / k_B T)},$$

k_B is Boltzmann's constant, e is the charge of an electron, $\tau = \mu E_F / e v_F^2$ is the electron scattering relaxation time, $v_F = 3 \times 10^6 ms^{-1}$ is the Fermi velocity of charge carriers in graphene, and the electron mobility is chosen conservatively as $\mu = 1 \times 10^4 cm^2(Vs)^{-1}$ [32]. We note that the weak localization of TE plasmons (i.e., at the considered doping, $q \sim nk_0 \ll k_F$; $k_0 = \omega/c$ is the vacuum wavenumber, c is the speed of light in vacuum, and n is the refractive index of the surrounding bulk) ensures that the local limit applies.

The frequency dependent real and imaginary parts of conductivity ($\sigma = \sigma' + i\sigma''$) in the spectral transition region are shown in Fig. 1 for several Fermi energies and at the temperatures (a) $T = 300$K (room) and (b) $T = 80$K (liquid nitrogen); the conductivity is normalized to the universal conductivity, $\sigma_u = e^2/4\hbar$ [8]. The real part of conductivity σ', which determines the optical loss in graphene, is evidently characterized by a shift from small ohmic loss in the Drude regime ($\Omega < 2$; $\Omega = \hbar\omega/E_F$ is the normalized frequency), to a frequency independent absorption $\sigma' = \sigma_u$ ($\Omega > 2$) induced by interband carrier transitions which become dominant as $\hbar\omega > 2E_F$. The effect of increased temperature or decreased Fermi

energy is apparent in Fig. 1 as a broadening of the transition region. A step-like dependence of σ' is approached for increasing E_F/k_BT; the $T = 0$K limit is achieved as $E_F/k_BT \to \infty$ ($E_F \gg k_BT$). An increase of E_F/k_BT simultaneously increases the depth of the minimum of σ'', and a singularity $\sigma''(\Omega \to 2) \to -\infty$ occurs in the $T = 0$K limit [37].
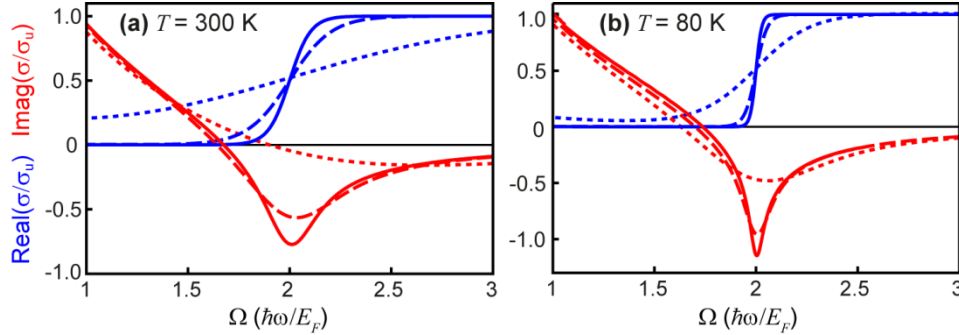

Fig. 1. Real (blue) and Imaginary (red) parts of the graphene conductivity in the spectral transition region at Fermi energies $E_F = 0.1$eV (dotted), 0.5eV (dashed), and 1eV (solid), and at temperatures $T = 300$K (a), and $T = 80$K (b). The electron mobility is $\mu = 1 \times 10^4$cm^2(Vs)$^{-1}$.

The efficiency of Otto excitation of TE plasmons in graphene will be shown below to increase with the plasmon effective index, $n_{\text{eff}} = q/k_0$. In the limiting case of a graphene layer immersed in a uniform medium of refractive index n, n_{eff} is given by the dispersion relation [37,45] $(n_{\text{eff}}^2 - n^2) = (i\sigma/2\varepsilon_0 c)^2$, where $\sigma'' < 0$; we refer to this as the symmetric, semi-infinite case. Analysis of this dispersion relation reveals that n_{eff} increases with the quantities $|\sigma''| - \sigma'$ and $|\sigma''|$, and thus the doping of graphene ($E_F/\hbar\omega$) should be chosen with a view to maximize these quantities. In this regard, for our study below we take the conductivity of a single-layer graphene to be $\sigma \sim 0.5\sigma_u - i\sigma_u$, which is achievable when $E_F \sim 0.5$eV and $T \sim 80$K.

3. Otto excitation of TE plasmons in single-layer graphene

We consider the Otto excitation scheme shown in Fig. 2(a): an effectively semi-infinite high-index dielectric medium (e.g., a coupling prism) with the refractive index $n_1 = 2$ is juxtaposed at the plane $x = 0$ with a semi-infinite low-index dielectric medium of refractive index $n_2 = 1.5$ in which a graphene layer with the sheet conductivity $\sigma = \sigma' + i\sigma''$ occupies the $x = d$ plane. A TE-polarized plane wave is incident onto the $n_1|n_2$ interface at an angle θ. The *ansatz* is made that the electric field in each medium $m = 1,2,3$ takes the form $\mathbf{E}^{(m)} = \hat{\mathbf{y}} E_m(x) \exp(iqz - i\omega t)$, where,

$$E_1(x) = A_1 \exp(ik_1 x) + B_1 \exp(-ik_1 x), x < 0;$$
$$E_2(x) = A_2 \exp(-\kappa[x-d]) + B_2 \exp(\kappa[x-d]), 0 < x < d; \quad (2)$$
$$E_3(x) = A_3 \exp(-\kappa[x-d]) + B_3 \exp(\kappa[x-d]), x > d.$$

Substituting the *ansatz* into the Helmholtz equation $\nabla^2\mathbf{E}^{(m)} + k_0^2\mathbf{E}^{(m)} = 0$ (where $k_0 = \omega/c$) we obtain $k_1 = \sqrt{k_0^2 n_1^2 - q^2}$ and $\kappa = \sqrt{q^2 - k_0^2 n_2^2}$, noting that $q = n_1 k_0 \sin(\theta)$ is the projection of the incident wavevector onto the z-axis. Assuming the harmonic time dependence $\exp(-i\omega t)$ of the magnetic field $\mathbf{H}$, substituting into the Maxwell curl equation $\nabla \times \mathbf{E} + \mu_0 \partial\mathbf{H}/\partial t = 0$, applying the electromagnetic boundary conditions $\hat{\mathbf{x}} \times (\mathbf{E}^{(m+1)} - \mathbf{E}^{(m)}) = 0$, $\hat{\mathbf{x}} \times (\mathbf{H}^{(m+1)} - \mathbf{H}^{(m)}) = \mathbf{K}$ at the interfaces, noting that $\mathbf{K}(x = 0) = 0$ and

$\mathbf{K}(x = d) = \sigma\mathbf{E}(x = d)$, and taking $B_3 = 0$ (i.e., absence of a reflected wave in medium 3), we obtain the reflection coefficient of the incident wave $R = |r|^2$ ($r = B_1/A_1$) with

$$r = -\frac{\kappa\left[\Lambda\cosh(\kappa d) + \kappa\sinh(\kappa d)\right] + ik_1\left[\kappa\cosh(\kappa d) + \Lambda\sinh(\kappa d)\right]}{\kappa\left[\Lambda\cosh(\kappa d) + \kappa\sinh(\kappa d)\right] - ik_1\left[\kappa\cosh(\kappa d) + \Lambda\sinh(\kappa d)\right]}, \quad (3)$$

where $\Lambda = \kappa - i\mu_0\omega\sigma$, and μ_0 is the vacuum magnetic permeability. We note that Eq. (3) can also be derived using the transmittance matrix technique [39,45].

In Fig. 2(b) we show the angular reflectance distribution $R(\theta)$ staggered for d from $d/\lambda = 0$ (bottom curve) to $d/\lambda = 30$ (top curve), and $\sigma \sim 0.5\sigma_u - i\sigma_u$. It can be seen that a sharp minimum in $R(\theta)$ emerges at the critical angle θ_c of the $n_1|n_2$ interface ($\theta_c = a\sin(n_2/n_1)$) when $d/\lambda > \approx 5$. The minimum becomes broadened as d increases while at the same time shifting to the right, yet remaining very close to θ_c within $\Delta\theta = \theta - \theta_c \sim 0.001$deg. The expected angular range of TE plasmon excitation can be approximated from the symmetric semi-infinite case (i.e., $d \to \infty$), $\theta_{TE} \sim a\sin(n_{eff}/n_1)$, which gives $\Delta\theta \sim 0.001$deg, thus suggesting that the reflection minimum could be a consequence of the excitation of TE plasmons. To eliminate the possibility that the reflection minimum is a trivial consequence of loss in the graphene layer (i.e., $\sigma' > 0$), we also plot $R(\theta, d/\lambda = 7)$ for when the incident wave is TM polarized (for both $\sigma'' > 0$ and $\sigma'' < 0$ – dashed curve Fig. 2(c); the derivation of the TM case is analogous to the above replacing $\mathbf{E}$ with $\mathbf{H}$ in Eq. (2)), and TE polarized with $\sigma'' > 0$. The evident absence of a distinct minimum in $R(\theta)$ in the vicinity of the critical angle except for when the incident wave is TE polarized and $\sigma'' < 0$ further suggests that the reflection minimum is solely due to the TE plasmon excitation.

Noting that in Fig. 2(b), $R_{max} \approx 0.966$ (at large angles $\theta > \theta_c$ $R_{max} \neq 1$ due to absorption in graphene), we find that the reflectance contrast does not exceed $\Delta R/R_{max} \sim 10\%$ ($\Delta R = R_{max} - R_{min}$, $R_{min} = \min[R(\theta \geq \theta_c)]$), and $R_{min} > 0$ for all d. Therefore critical coupling [52,53] of the incident wave to the TE plasmon (which would correspond to $R_{min} = 0$) is not achieved. Furthermore, noting the extremely narrow angular width of the reflection minimum that is $\delta\theta < 0.001$deg, which exceeds the angular resolution limit of typical SPP detectors (see for example Table 2 in [54], and [55]), the Otto excitation of TE plasmons in the considered single-layer graphene at $T = 80$K would be a challenge to detect experimentally.

A theoretical understanding of the dispersive properties of TE plasmons supported by graphene in an Otto configuration will suggest routes toward loosening the experimental conditions required for their experimental detection. To this end we solve the dispersion relation of leaky TE plasmons in the asymmetric three-layer system of Fig. 2(a). The dispersion relation is obtained on setting $A_1, B_3 = 0$ in Eq. (2), substituting into the boundary conditions on $\mathbf{E}$ and $\mathbf{H}$, and then setting the resulting 4×4 determinant of coefficients $B_1, A_2,, B_2, A_3$ equal to zero, thus arriving at:

$$\exp(-2\kappa d) = \frac{k_1 + i\kappa}{k_1 - i\kappa}\frac{i2\kappa + \omega\mu_0\sigma}{\omega\mu_0\sigma}. \quad (4)$$

Equation (4) is solved numerically for complex $q = q' + iq''$ under the condition that $\mathrm{Re}(\kappa) \geq 0$ which ensures that the plasmon electric field is exponentially bound to the graphene layer and leaks only into propagating modes of medium 1. The expected angle of excitation of the leaky TE plasmon, θ_{TE}, is obtained from the phase matching condition $q' = n_1 k_0\sin(\theta_{TE})$ [44,45].
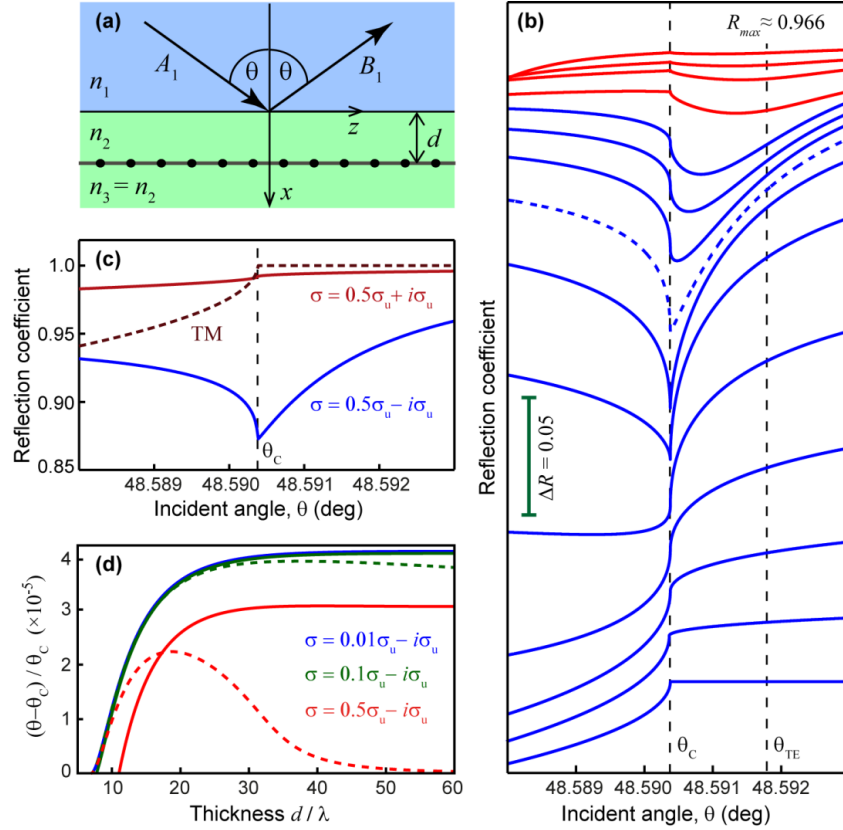
Fig. 2. (a) Schematic of the Otto excitation structure. A_1 and B_1 are the electric field amplitudes of the incident and reflected TE (y-polarized) plane waves, θ is the angle of incidence and reflection, d is the thickness of the film between the $n_1|n_2$ interface and the graphene layer, and n_1 (n_2) is the refractive index of the high-index (low-index) medium. (b) Staggered plot of angular reflectance distributions $R(\theta)$ at $d/\lambda = 0, 1, 2, 3, 4, 5, 6, 7, 8, 9, 10, 15, 20, 25, 30$ (curves from bottom-to-top). We note that $R(\theta = 48.593) \approx R_{max} = 0.966$, and the actual reflectance is indicated by the green scale bar. The dashed blue line coincides with the cutoff d, $d_{cut}/\lambda \approx 7$. The graphene conductivity is $\sigma = 0.5\sigma_u - i\sigma_u$. (c) $R(\theta)$ for case of TE (solid curves) and TM (dashed curve) incident wave polarization and positive/negative sign of $\mathrm{Im}(\sigma)$; $\sigma = 0.5\sigma_u \pm i\sigma_u$ and $d/\lambda = 7$. (d) d-dependence of normalized angular deviation of θ_{TE} (solid curves) and θ_{min} (dashed curves) from the critical angle θ_c.

In Fig. 2(d) we plot the normalized deviation from the critical angle of $\theta_{TE}(d)$ (solid curves), and also for the angle θ_{Rmin} (dashed curves) corresponding to the minimum of $R(\theta \geq \theta_c)$ (i.e., $R(\theta_{Rmin}) = R_{min}$), for the conductivity $\sigma = 0.5\sigma_u - i\sigma_u$ (red curves). To observe contrasting behavior, we also show data for two experimentally challenging (e.g. very-low temperature) conductivities exhibiting smaller internal loss σ': $\sigma = 0.1\sigma_u - i\sigma_u$ (green curves) and $\sigma = 0.01\sigma_u - i\sigma_u$ (blue curves). Firstly, we note that each curve $\theta_{TE}(d)$ asymptotically approaches a fixed value at large d, which expectedly corresponds exactly to the wavenumber of TE plasmons in the symmetric semi-infinite structure with refractive index n_2. Secondly, we note that all curves $\theta_{TE}(d)$ collapse to the critical angle θ_c at a particular value $d = d_{cut}$ – see also the dashed curve in Fig. 2(b) corresponding to $d/\lambda = 7$. This value of d constitutes a cutoff at which the electric field of the TE plasmon becomes completely delocalized (i.e., $\kappa(d = d_{cut}) = 0$) and leaks into propagating modes of medium 3 (see also Fig. 3(c)). The cutoff can be easily obtained from Eq. (4) taking $\kappa \to 0$ and Taylor expanding the LHS to first order. In the limit of zero loss ($\sigma' = 0$) and when $k_1 \gg \omega\mu_0|\sigma''|$ we obtain $d_{cut}/\lambda \approx c\varepsilon_0/(2\pi|\sigma''|)$ which gives $d_{cut}/\lambda \approx 7$

when $\sigma'' = -\sigma_u$, and matches very well with the distance at which blue and green curves in Fig. 2(d) collapse to critical angle, i.e. those corresponding to small internal loss ($\sigma' << |\sigma''|$).

Thirdly, while we note excellent quantitative agreement between $\theta_{TE}(d)$ and $\theta_{Rmin}(d)$ to within < 0.01% at each of the considered conductivities, there is evident mismatch when $\sigma' = 0.5\sigma_u$ (red solid and dashed curves in Fig. 2(d)). This is related to strong under-coupling [53] of the incident wave to the TE plasmon at large internal loss. To illustrate this, in Fig. 3(a) we plot the d-dependent internal loss coefficient q_{int}'' (solid curves) and radiative loss coefficient q_{rad}'' (dashed curve) of the TE plasmon at each of the three considered conductivities; the data for each conductivity is plotted over the domain $d \geq d_{cut}$. The quantity q_{rad}'' is obtained from the solution of Eq. (4) after setting $\sigma' = 0$ in which case $q_{rad}'' = q''$ i.e., the only loss mechanism is radiative loss. The quantity q_{int}'' is obtained on introducing $\sigma' \neq 0$, solving Eq. (4), and taking $q_{int}'' = q'' - q_{rad}''$. Interestingly, we see that when the conductivity takes the realistic value $\sigma = 0.5\sigma_u - i\sigma_u$, at all $d > d_{cut}$, the internal loss is several orders of magnitude greater than the radiative loss, which is far from the critical coupling regime; critical coupling occurring when $q_{int}'' = q_{rad}''$ [52]. Considering that the radiative loss is reciprocal to the radiative coupling gain, we see that the TE plasmon is in fact strongly under-coupled. At the same time, it is interesting to note that cumulatively (i.e., internal plus radiative loss), the plasmon itself exhibits very low propagation loss, with a normalized (to the plasmon wavelength λ_p) propagation length $l \approx 1/q'' \sim 1000\lambda_p$. The low loss of the plasmon is responsible for the narrow angular width of the minimum in $R(\theta)$ [44], yet the existence of a large cutoff thickness d_{cut} forbids the incident wave from effectively driving the plasmon.
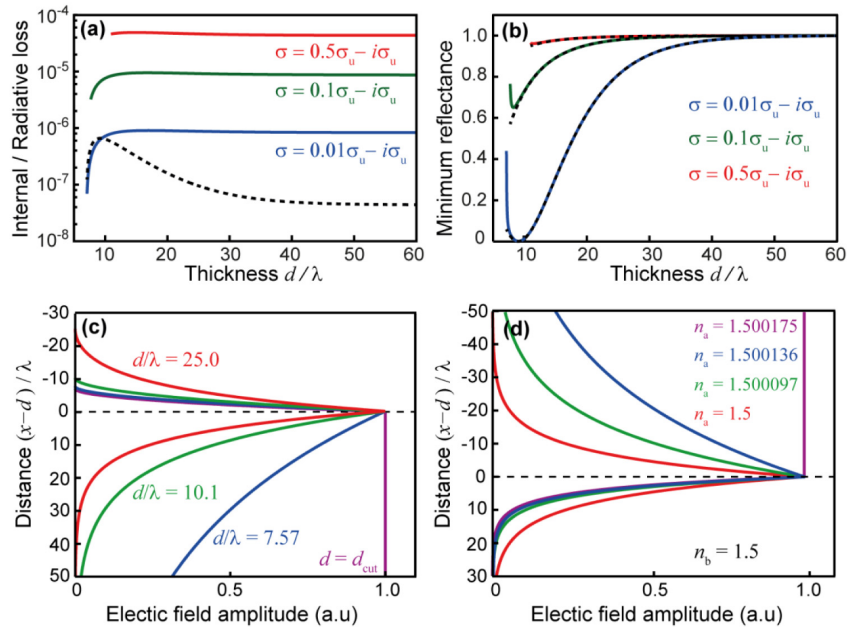

Fig. 3. (a) d-dependence of TE plasmon internal (q_{int}''; colored curves) and radiative (q_{rad}''; dashed black curve) propagation loss. (b) d-dependence of minimum reflectance $R(\theta_{min})$ (solid curves) and $R(\theta_{TE})$ (black dashed curves). Colors in (a,b) indicate conductivities as noted. (c,d) Electric field intensity profile of asymmetric TE plasmons illustrating cutoff behavior: (c) Otto configuration at indicated d. (d) Asymmetric semi-infinite structure at indicated values of n_a and n_b. The dashed line $x = 0$ marks the position of the graphene layer.

We expect that increased coupling of the incident wave to the TE plasmon could be achieved by reducing the internal loss (σ') of the graphene (and thus, q_{int}''), such that the plasmon internal loss becomes comparable to the radiative loss – this is demonstrated by the

green and blue curves in Figs. 3(a) and 3(b), corresponding respectively to $\sigma' = 0.1\sigma_u$ and $\sigma' = 0.01\sigma_u$. For small internal loss such as $\sigma' = 0.01\sigma_u$, the critical coupling condition [52,53], for which the internal loss becomes equal to the radiative loss, can be satisfied (see blue curve intersecting with black dashed curve in Fig. 3(a)), and $\theta_{TE}(d)$ and $\theta_{Rmin}(d)$ almost perfectly match (Fig. 2(d)). Naturally, we expect a zero in $R(\theta)$ when $q_{int}'' = q_{rad}''$ is satisfied; this is illustrated by the blue curve in Fig. 3(b). It is evident from Fig. 3 (a) that when σ' is further reduced, the radiative and internal plasmon loss will become comparable or equal at larger values of the film thickness d, and thus evidence of coupling of the incident wave to the TE plasmon is seen at larger film thickness (see Fig. 3 (b)). On the other hand, in the lossless case ($\sigma' = 0$), the evidence of TE plasmon coupling is absent from the angular reflectance distribution since there is no light absorption in the graphene layer. Thus, decreasing the internal loss of graphene significantly increases coupling between the plasmon and incident wave, resulting in strong reduction of the reflectance at the TE plasmon resonance. It is unusual that, although the plasmon itself exhibits extremely weak internal losses, a route to its more convenient experimental detection (i.e., increased contrast of the reflectance minimum) would be to further reduce the internal loss of the single-layer graphene. However, to do so would require the cooling of the graphene to very low temperatures.

To obtain insight into the cutoff dynamics of Otto excited TE plasmons, in Fig. 3(c) we show the plasmon electric field intensity distribution $|E_{2,3}(x - d)|^2$ at several values of d, as determined from substituting $q(d) = q' + iq''$ (i.e., with q obtained from Eq. (4)) into the boundary conditions with $A_1, B_3 = 0$ and normalizing so that $A_3 = 1$. When $d \gg d_{cut}$, we observe an almost symmetric field distribution (about $x = d$) which approaches that of the TE plasmon of the semi-infinite symmetric structure. As $d \rightarrow d_{cut}$ the field becomes increasingly asymmetric, rapidly delocalizing from the graphene layer in medium 3, while slowly becoming more localized in medium 2. The cutoff $d = d_{cut}$ corresponds to complete delocalization of the field and leakage of the plasmon into propagating waves in medium 3 (in the positive-x direction). To contrast, we also show the electric field distribution of TE plasmons supported by a graphene sheet (at $x = d$) sandwiched between two semi-infinite dielectrics with the respective refractive indices n_a ($x < d$) and n_b ($x > d$), referred to as the asymmetric semi-infinite structure – Fig. 3(d). We note that the cutoff behavior in the asymmetric semi-infinite structure holds qualitative similarity to that of the Otto structure, except comparing each case shows that the plasmon becomes delocalized toward opposite sides of the graphene layer (i.e., toward or away the side containing the high index medium).

The cutoff dynamics of TE plasmons in the Otto configuration are further revealed on calculating the z-component of power flow in medium 1, 2 and 3 given respectively by

$$P^{(1)} = \int_{-\infty}^{0} S_z^{(1)} dx \,, \ P^{(2)} = \int_{0}^{d} S_z^{(2)} dx \ \text{and} \ P^{(3)} = \int_{d}^{\infty} S_z^{(3)} dx \ \text{where} \ S^{(m)} = (1/2)\text{Re}[\hat{\mathbf{z}} \cdot (\mathbf{E}^{(m)} \times \mathbf{H}^{(m)*})] \ \text{is}$$

the time-averaged z-component of Poynting vector in medium m, and the electric fields are given by Eq. (2) with $A_1, B_3 = 0$. In the limit of weak-leakage of the plasmon ($q'' \ll q'$), we have $P^{(1)} \ll P^{(2)} + P^{(3)}$ (since $P^{(1)}$ contains only the leakage wave prior to the cutoff), and $P^{(2)} + P^{(3)} \approx C$ where C is a d-independent constant. We find in the limit $\kappa \rightarrow 0$ that $P^{(2)} \approx |A_3|^2 d$, and $P^{(3)} \approx |A_3|^2/2\kappa$. Thus we see that as the cutoff (i.e., corresponding to $\kappa \rightarrow 0$) is approached, the plasmon amplitude (A_3) approaches zero (to ensure that C is finite), and $P^{(2)}/P^{(3)} \approx 2\kappa d \rightarrow 0$, showing that the plasmon energy is mostly found in medium 3 ($x > d$). Furthermore, the power cutoff dynamics are independent of the optical contrast across the interface separating medium 1 from 2 (i.e., $\Delta n = n_1 - n_2$), and depend only on n_2 (recalling that $\kappa = \sqrt{q^2 - k_0^2 n_2^2}$), whereas the cutoff behavior in the semi-infinite anti-symmetric structure is very sensitive to the optical contrast [40]; the former is also consistent with the absence of the optical contrast from the expression for the cutoff thickness ($d_{cut}/\lambda \approx c\varepsilon_0/(2\pi|\sigma''|)$). On the other hand, we find that reducing the optical contrast can increase the coupling efficiency of the incident wave to

the TE plasmon owing to increased penetration of the totally reflected incident beam (i.e., for $\theta > \theta_C$) into medium 2. We also point out that the cutoff itself, inversely proportional to $|\sigma''|$, suggests a second route (besides reducing the internal loss) to more convenient detection of TE plasmons in graphene. Indeed, increasing $|\sigma''|$ will reduce the cutoff thickness and allow increased coupling between the incident wave and the TE plasmon. This is demonstrated in Fig. 4 (a), where we plot $R(\theta_{min})$ for increasing values of $|\sigma''|$ while keeping the internal loss fixed at $\sigma' = 0.5\sigma_u$ (similarly to Fig. 3(b), each curve is terminated at the respective values of $d = d_{cut}$). A significant reduction of the reflectance reveals enhanced coupling of the incident wave to the TE plasmon at increasing values of $|\sigma''|$, including critical coupling for when $\sigma'' = -8\sigma_u$; the cutoff prevents the critical coupling condition from being satisfied when $|\sigma''| < \approx 8\sigma_u$. The TE coupling enhancement is further demonstrated in Fig. 4(b) which shows the angular reflectance distribution at those values of d providing the minimum reflectance (as obtained from Fig. 4(a)). Yet considering that $|\sigma''| > 1$ is difficult to achieve in practice except at very low temperature, in section 4 we suggest and demonstrate that multi-layer graphene stacks (see for example [27,45,48]) is a way to increase the effective conductivity of graphene toward providing less strict experimental conditions for the detection of TE plasmons.
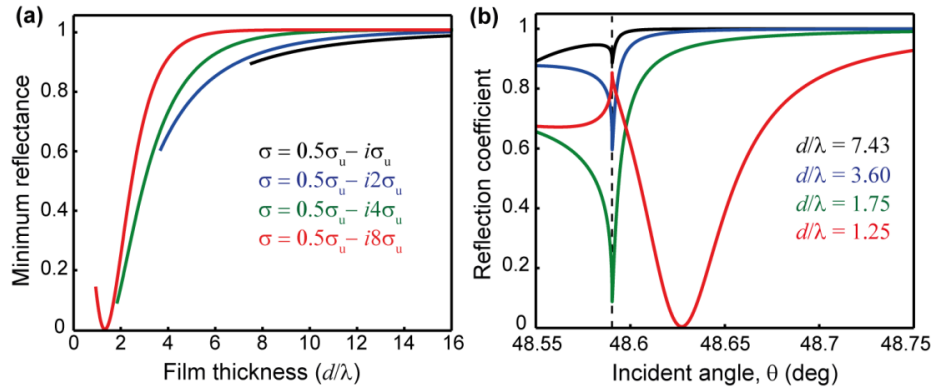

Fig. 4. (a) d-dependence of minimum reflectance $R(\theta_{min})$. (b) Angular reflectance distributions $R(\theta)$ corresponding to indicated values of d. Colors in (a,b) indicate conductivities as given in inset of (a). All other parameters are the same as for Fig. 2(b).

Finally, we note that it was recently predicted that TE plasmons supported in an optical cavity exhibit a cutoff with respect to the cavity width [43]. From this context, our results demonstrate that a TE plasmon cutoff is exhibited not only in an enclosed cavity but also when the TE plasmon is attempted to be confined on only one side by a high index medium.

4. Multi-layer graphene stacks toward detection of TE plasmons at room temperature

In section 3 we predicted that the Otto excitation of TE plasmons in a single-layer graphene can lead to a minimum in the angular reflectance distribution at the critical angle with a contrast $\Delta R/R_{max} \sim 10\%$, although which would require a very high angular resolution exceeding ~0.001deg to experimentally detect. In this regard, we seek a means to increase the angular width and depth of the reflection minimum to facilitate the feasible experimental detection of TE plasmons in graphene. In this section we propose that stacking multiple single-layer graphenes [27,47] could provide both a widening and deepening of the reflectance minimum owing to an effective increase of the graphene conductivity. For example, in graphene insulator stacks [27,48] or multi-layer graphene obtained from layer-by-layer transfer of single-layer graphenes [47], electronic decoupling between neighboring graphene layers provides an effective conductivity increase according to $\sigma_N = N\sigma$ [27,47] as the distance between neighboring layers approaches zero; N is the number of single-layer graphenes in the stack, σ is the sheet conductivity of a single-layer graphene, and σ_N is the

effective sheet conductivity of the graphene multi-layer stack. We note that a random crystalline orientation between neighboring graphene layers [27,47] provides the electronic decoupling [46] (and $N\sigma$ behavior), while for bi-layer or few layer graphene, the expression for conductivity becomes increasingly complicated (see for example [38]).

We start at an Otto configuration with two single-layer graphenes (a two layer system) – the structure is the same as Fig. 1(a) except with an additional single-layer graphene inserted at the plane $x = d + \Delta$. Insight into the TE plasmon dynamics as the structural transition is made from the two-isolated-layer system (i.e., $\Delta > 0$) to the two-layer-stack (i.e., as $\Delta \rightarrow 0$) is obtained by solving the dispersion equation of TE plasmons supported by the two layer system. The dispersion equation is derived in determinant form following the same method in section 2 after inserting an additional layer ($d < x < d + \Delta$) and boundary condition (i.e., at the additional graphene layer) at $x = d + \Delta$. Expectedly, we find that the dispersion equation has two solutions corresponding to an even or odd coupled mode (i.e., with equal or opposing sign of electric field at either graphene layer) each comprising the even or odd coupling between the TE plasmons supported by each single layer system (i.e., one with a single-layer graphene only at $x = d$, and the other only at $x = d + \Delta$).
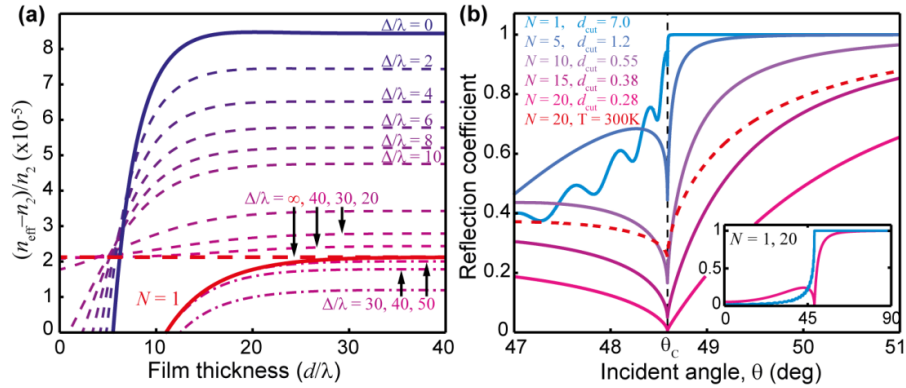

Fig. 5. (a) d-dependent normalized effective index deviation of even (dashed) and odd (dot-dashed) TE plasmon coupled-modes of an Otto system with two single-layer graphenes at indicated values of the inter-layer distance, Δ. The conductivity of each single-layer graphene is $\sigma \sim 0.5\sigma_u - i\sigma_u$. The solid blue and red curves correspond to a single layer Otto system with the graphene conductivity $\sigma \sim 2(0.5\sigma_u - i\sigma_u)$, and $\sigma \sim 0.5\sigma_u - i\sigma_u$, respectively. The thick red dashed curve corresponds to the semi-infinite symmetric structure. (b) Angular reflectance distributions $R(\theta)$ for an Otto system with an N-layer graphene stack ($\Delta/\lambda = 0.001$) at respective $d = d_{cut}(N)$ and with $\sigma \sim 0.5\sigma_u - i\sigma_u$ (solid curves; $T \sim 80K$) and $\sigma \sim 0.5\sigma_u - i0.5\sigma_u$ (dashed red curve; $T \sim 300K$). Inset: wide-angle comparison of single-layer and 20-layer reflectance distributions over $0 < \theta < 90$ (deg) with $\sigma \sim 0.5\sigma_u - i\sigma_u$.

The d-dependence of the deviation of the TE coupled-mode plasmon effective index (with respect to, and normalized to the bulk effective index: $(n_{eff}-n_2)/n_2$, which equals to zero at $d = d_{cut}$) of both even (dashed) and odd (dot-dashed) mode solutions is shown in Fig. 5(a) at indicated values of normalized inter-layer separation (Δ/λ), and when the single-layer graphene conductivity is fixed at $\sigma = 0.5\sigma_u - i\sigma_u$. As Δ increases, we see that the odd mode effective index converges exactly to that of the plasmon supported by the single layer system (marked $N = 1$, thick red solid line), in which case the plasmon field is bound only to the upper graphene layer (i.e., at $x = d$). For the odd mode, coupling induced perturbation of the effective index (evident for smaller values of Δ) rapidly increase d_{cut} (the d/λ-intercept in Fig. 5(a)) which would significantly reduce coupling of an incident wave to the odd TE plasmon mode. Thus we conclude that the odd TE mode would likely be experimentally undetectable at the considered single-layer graphene conductivity. In contrast, modal coupling rapidly increases the effective index of the even TE plasmon mode, starting at that of the TE plasmon of the isolated lower graphene layer (see the thick red dashed curve in Fig. 5(a), which

corresponds to the symmetric semi-infinite structure), and in the limit that $\Delta \rightarrow 0$, converging to that of a single layer system with an effective conductivity $\sigma_2 = 2\sigma$ and a halved (i.e., as compared to the single-layer case) cutoff thickness $d_{cut}/\lambda = 3.5$. As we predicted in section 3, a decreased cutoff thickness (at increased $|\sigma''|$) provides increased coupling of the TE plasmon to the incident wave.

To demonstrate increased coupling of an incident wave to TE plasmons in N-layer graphene stacks, in Fig. 5(b) we plot the angular reflectance distribution $R(\theta)$ about the critical angle (vertical dashed line) for when $d = d_{cut}$ at the respective values of N (as indicated in the figure). These curves are obtained from the transmittance matrix method [39,45] with the inter-layer spacing $\Delta/\lambda = 0.001$. It is immediately evident that the reflection minimum significantly widens and deepens as the numbers of layers in the graphene stack (N) increases, even to the extent that critical coupling is achieved (i.e., $R(\theta_c) \approx 0$) when $N = 20$. The angular width of the reflection minimum is increased by two orders of magnitude from $\Delta\theta \sim 0.001$deg in the single layer case to $\Delta\theta \sim 0.1$deg when $N \sim 10$, providing for much easier experimental detection (see also inset of Fig. 5(b)). We also show an example case of a 20-layer graphene stack at room temperature ($T = 300$K) for which we have taken the single layer graphene conductivity as $\sigma = 0.5\sigma_u - 0.5i\sigma_u$ (see Fig. 1(a)). Interestingly, an appreciable contrast of the reflection minimum ($\Delta R/R_{max} \approx 70\%$) is obtained while preserving the broad angular width. These results are therefore promising toward the experimental detection of TE plasmons in graphene including at room temperature.

5. Conclusion

We investigated an Otto configuration as a route to the experimental detection of TE plasmons in graphene. From solution of their dispersion equation, we demonstrated that TE plasmons supported by graphene in an Otto configuration exhibit a cutoff at a particular thickness of the film between the graphene layer and the coupling prism. While the TE plasmon exhibits very weak internal and radiative losses, the existence of the cutoff was shown to prevent its efficient coupling to an incident wave. These two factors produce a minimum in the angular reflectance distribution which is both low contrast ($\Delta R/R_{max} < 10\%$) and of exceptionally narrow angular width ($\Delta\theta \sim 0.001$deg), hindering the experimental detection of TE plasmons in single-layer graphene at finite temperatures. To address this issue, we proposed the Otto excitation of TE plasmons in a multi-layer stack of single-layer graphenes. Owing to the effective increase of the graphene conductivity by a factor equal to the number of layers (i.e., $\sigma_N = N\sigma$), we demonstrated significantly increased coupling of TE plasmons to an incident wave, including orders-of-magnitude increase in the angular width and reflectance contrast of the TE plasmon resonance. Our results suggest that an Otto scheme with a graphene multi-layer stack provides the first recognized platform for the feasible detection of TE plasmons in graphene at room temperature. Experimental detection of TE plasmons in graphene is of significant fundamental importance and the experimental implementation of the suggested Otto scheme is to be presented in a future work. We foresee that our proposed scheme could provide a realistic platform for a new type of SPP detector based on the narrow angular width of the TE plasmon resonance.